Unraveled mechanisms in energy production from bioresources using steam gasification

Lina Maria Romero Millan, Fabio Emiro Sierra Vargas, Ange Nzihou

Unraveled mechanisms in energy production from bioresources using steam gasification

Lina María Romero Millán [a,b,*], Fabio Emiro Sierra Vargas [b], Ange Nzihou [a]

[a] Université de Toulouse, IMT Mines Albi, CNRS, Centre RAPSODEE, Campus Jarlard, Route de Teillet, F.81013 Albi Cedex 09, France
[b] Universidad Nacional de Colombia – Sede Bogotá, Facultad de Ingeniería, Ciudad Universitaria, Bogotá, Colombia

Keywords:
Lignocellulosic biomass
Steam gasification
Catalytic mechanism
Inorganic composition
Product yield
Gas efficiency

A B S T R A C T

Lignocellulosic agrowastes are one of the most abundant and inexpensive bioresources on earth. However, they comprise a wide range of materials with different organic and inorganic composition that may influence their performance in energy applications. Here, we analyze the impact of inherent inorganics on the steam gasification performance of bioresources, using an approach combining the analysis of the gasification reaction mechanisms, and the assessment of the process product distribution and energy balance. We proved that the inorganic ratio K/(Si + P) is a valuable indicator of the biomass gasification reactivity and product yield. Under the same experimental conditions, samples with K/(Si + P) higher than 1 followed a catalytic gasification behavior, resulting in higher gas yields and process gas efficiencies in comparison to samples with K/(Si + P) below 1. This work is expected to bring new insights in the field and could facilitate the adaptation of the process parameters to the feedstock characteristics and the application requirements.

1. Introduction

Each year, billion tons of agricultural and agroindustrial wastes are generated all around the world, representing one of the most abundant and inexpensive bioresources on earth [1]. Being widely available, agrowastes constitute a valuable and renewable source of energy in developed and developing countries, in the framework of an environmentally sustainable approach, representing more than 7 million terajoules of energy, or the equivalent of more than 7.5 billion barrels of diesel [2–5]. Among the existing agrowaste conversion pathways, steam gasification is particularly interesting, as it allows the production of high heating value fuel gases (10 and 18 MJ/m^3), for the generation of heat or power [6–8], as well as the synthesis of advanced chemicals [9–11]. However, the sustainable use of these bioresources for energy production needs to overcome different challenges related to their variability. In particular, the volume of residues generated from agricultural and agroindustrial activities is not constant throughout the year, and is regularly determined by the seasonality of crops. Therefore, the associated gasification facilities should work intermittently, or employ multiple kinds of residues with heterogeneous characteristics.

Along with the reactor configuration and the process operating conditions like temperature and steam flowrate, the characteristics of the feedstock may also impact the performance of gasification, and particularly, the produced gas composition and yield [12–14]. Regarding the steam gasification product distribution and gas composition, several studies related to different kinds of lignocellulosic feedstocks have been developed [15–17], dealing with the analysis of residues individually, without comparing different materials. A few approaches working with several feedstocks described some divergences in the gas production rate and composition during gasification, attributed to the samples ash content and composition, volatile matter, particle porosity, or particle size, without defining the mechanisms associated with the described behavior [12,18,19].

In general, lignocellulosic materials are a complex mixture of natural polymers, mainly hemicellulose, cellulose, and lignin, tightly bonded by physical and chemical interactions [20,21]. They may have different proportions of the constituent polymers depending on the plant species, origin, and age, as well as several inorganic elements present in their structure [22]. In this regard, it has been proven that the biomass gasification reactivity may depend on the sample morphology, structure, and composition [23,24]. Among these parameters, the biomass inherent inorganic composition has been identified as the most influencing one [25–27]. In particular, alkali and alkali earth metals (AAEM) like K, Na, Ca and Mg, are related to a catalytic effect on biomass

* Corresponding author at: Université de Toulouse, IMT Mines Albi, RAPSODEE CNRS, UMR 5302, Campus Jarlard, 81013 Albi Cedex 09, France.
E-mail addresses: lina.romero_millan@mines-albi.fr (L.M. Romero Millán), fesierrav@unal.edu.co (F.E. Sierra Vargas), ange.nzihou@mines-albi.fr (A. Nzihou).

gasification [28–31]. Among these elements, K has been reported to be the most active species for steam and CO_2 gasification of charcoal and biomass [28,29]. In contrast, Si, Al or P may inhibit this catalytic effect, as they tend to react with AAEM [32,33]. In accordance, the understanding of the influence of the feedstock characteristics on the steam gasification behavior and product distribution is a fundamental issue to further develop steam gasification as a viable process for energy applications.

In this work, we elucidated the gasification behavior and product distribution of lignocellulosic agrowastes, as a function of their composition. Thus, coconut shells (CS), bamboo guadua (BG), and oil palm shells (OPS) were strategically selected as raw materials, considering their different macromolecular structure and inorganic composition. The steam gasification process was analyzed for the raw samples and selected blends, with a focus on the gas production and process efficiency. The characterization of the gasification solid by-product supported the description of the gasification mechanism of the selected samples. The approach and results developed in this paper give a point of reference to properly adapt the process parameters of gasification facilities to the feedstock characteristics and application. They constitute a contribution beyond the state-of-the-art in the domain of biomass to energy.

2. Materials and methods

2.1. Biomass samples

Three different lignocellulosic feedstocks were selected for this study. Coconut shells (CS), bamboo guadua (BG), and oil palm shells (OPS) were strategically chosen as raw materials, considering their different macromolecular structure and inorganic composition, detailed in a previous work [34], and summarized in Table 1. The elemental analysis (CHNS) of the three samples showed very similar results. In contrast, the comparison of their macromolecular and inorganic composition revealed remarkable differences. Regarding the macromolecular composition, coconut shells (CS) and oil palm shells (OPS), as endocarp residues, have high lignin content in comparison to bamboo guadua (BG), mainly constituted of cellulose. In relation to the inorganic composition, coconut shells main inorganic constituents are K, Ca, and Na, while oil palm shells and bamboo guadua are principally composed of Si and P. This choice might give an interesting outlook into the impact of biomass composition on the gasification behavior and product distribution of a wide range of lignocellulosic feedstocks. Moreover, to elucidate the impact of intermediate organic and inorganic compositions between the three selected samples, bi-component biomass blends were also analyzed using different proportions (90%CS-10%OPS, 90% CS-10%BG, 50%CS-50%OPS, and 50%CS-50%BG in wt. %). The raw feedstocks were milled and sieved to a particle size between 2 and 4 mm before the gasification experiments.

2.2. Steam gasification experiments

Gasification experiments were performed using a semi continuous laboratory scale fluidized bed gasifier. With a height of 60 cm and an internal diameter of 6 cm, the stainless steel reactor was externally heated with an electrical furnace. A porous disk in the bottom held the biomass samples, and allowed the gasification atmosphere to pass through. The thermal regulation was ensured by an Eurotherm controller connected to a thermocouple in the center of the reactor. The reacting agent (steam) and fluidizing inert gas (N_2) were regulated by calibrated flow mass controllers. At the exit of the reactor, a gas conditioning unit based on the tar protocol [35], allowed the condensation of tars and steam using a series of 7 impinger bottles. After the condensation train, a gas meter measured the volume of the produced gas (see Fig. 1). For all the experiments, 80 g of biomass were used. The minimum flow required to fluidize the biomass bed was experimentally determined by monitoring the pressure drop through the particle bed, while increasing the N_2 flow rate. A liquid column manometer connected at the top and the bottom of the reactor (acetylene tetrabromide) was used for this purpose. The pressure drop increases with the gas flow while the fluidization condition is not reached. Once the particle bed is fluidized, the pressure drop stabilizes. In accordance, it was observed that from a total flow rate of 0.6 m^3/h (Minimum fluidization velocity V_{mf} : 0.06 m/s), the biomass bed was fluidized. The sample inside the reactor was heated to the gasification temperature at a rate of 20 °C/min, under nitrogen. When the gasification temperature was reached (from 750 °C to 850 °C), the atmosphere was switched to a mixture of H_2O/N_2 (100 g/h of steam − 30% of steam in the gasifying agent) and was maintained during all the gasification stage (holding time at the gasification temperature from 1 h to 3 h). The total flow rate at the inlet of the reactor was 0.7 m^3/h for all the experiments (V: 0.07 m/s, V/V_{mf}: 1.2). Every 5 min, the gas volume produced was registered, and gas samples were taken using Tedlar® bags to analyze their composition. For this purpose, a micro-GC (MyGC Agilent) was used. The gas heating value was calculated from the CO, H_2, CH_4 and C_nH_m measured fractions. After each test, the reactor was cooled down to room temperature under N_2. The remaining char was collected and weighted, as well as the impinger bottles and pipes, to determine the quantity of water and tars condensed, and perform mass balances. For this purpose, the condensation train impinger bottles and pipes were also weighted prior to each

Table 1
Organic and inorganic composition of the three selected samples.

		Coconut shells (CS)	Bamboo guadua (BG)	Oil palm shells (OPS)
Elemental Analysis [a] (wt. % dry ash free)	C	46.8 ± 0.2	46.7 ± 0.2	46.7 ± 0.2
	H	5.8 ± 0.1	6.5 ± 0.1	6.5 ± 0.1
	O*	47.1 ± 0.1	46.2 ± 0.1	46.2 ± 0.1
	N	0.3 ± 0.1	0.6 ± 0.1	0.6 ± 0.1
	O/C	0.7 ± 0.1	0.7 ± 0.1	0.7 ± 0.1
	H/C	1.5 ± 0.1	1.7 ± 0.1	1.7 ± 0.1
Proximate analysis [b] (wt. % dry basis)	Volatile Matter	79.5 ± 0.3	77.2 ± 0.3	77.2 ± 0.3
	Fixed Carbon*	19.0 ± 0.2	20.9 ± 0.3	20.9 ± 0.3
	Ash	1.4 ± 0.1	1.7 ± 0.2	1.7 ± 0.2
Macromolecular composition [c] (wt. % dry ash free)	Cellulose	32.5	53.9	30.4
	Hemicellulose	20.5	13.5	12.7
	Lignin	36.5	25.1	49.8
High heating value [d] (MJ/kg)	HHV	18.7 ± 0.3	19.6 ± 0.2	19.6 ± 0.2
Inorganic composition [e] (mg/kg dry basis)	Al	262 ± 8	243 ± 34	1 500 ± 22
	Ca	391 ± 73	441 ± 99	54 ± 6
	Fe	160 ± 28	116 ± 17	107 ± 4
	K	2 808 ± 44	5 360 ± 85	1 006 ± 15
	Mg	170 ± 15	173 ± 10	135 ± 3
	Na	330 ± 11	30 ± 0.8	15 ± 0.5
	P	397 ± 40	829 ± 62	270 ± 7
	Si	309 ± 43	19 372 ± 354	5 600 ± 39

* Calculated by difference.
[a] Determined using a Themoquest NA 200 elemental analyzer. Standard EN ISO 16948.
[b] Calculated according to standards EN ISO 18134–3, EN ISO 18123, and EN ISO 18122.
[c] From [59].
[d] Determined using an IKA C 5000 automated bomb calorimeter, according to EN ISO 18125.
[e] Determined using inductively coupled plasma optical emission spectrometer (ICP-OES), according to EN 16967.

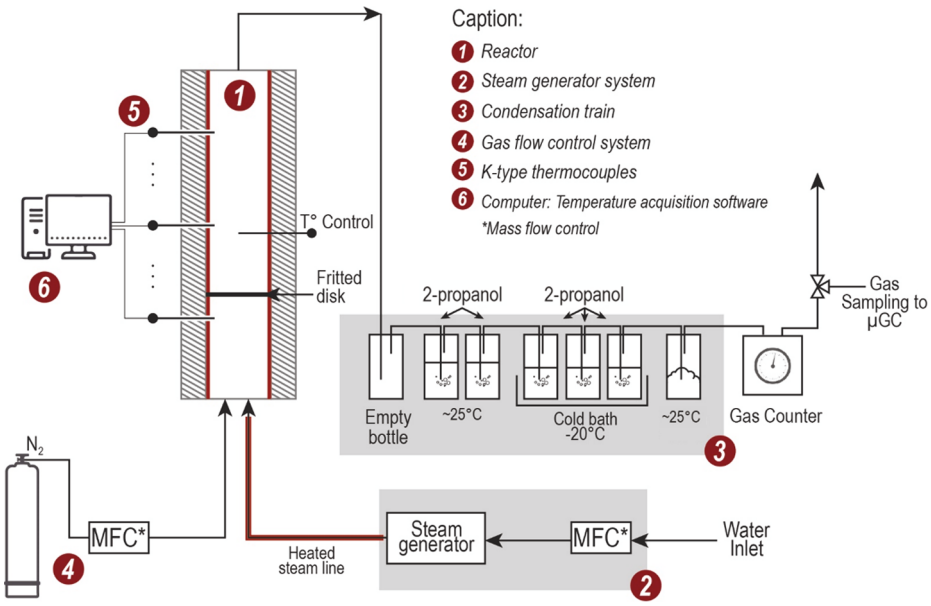

Fig. 1. Schematic diagram of the gasification experimental setup.

test. Pyrolysis tests were carried out to assess the gas, solid and liquid yield at the end of the heating period (pyrolysis stage), for each gasification temperature. Pyrolysis and gasification tests were carried out twice. The repeatability was found to be satisfactory as the standard deviation of the gas composition was below 3% (for all the measured gases), and the gas production below 10%, for all the analyzed samples. Also, the standard deviation of the produced char yield was below 3% for all the samples.

2.3. Product mass yield and energy fraction

The mass balance for each experimental condition was calculated from the gravimetrically measured solid (char) and liquid yields (tar + water), and the registered gas volume production and composition. As the last bottles of the condensation train are placed in a −20 °C cold bath, it was considered that the 2-propanol in the impingers is not volatilized during the experiment, and then, the liquid yield was determined from the mass difference between the condensation train before and after the test.

Considering that the nitrogen flow supplied to the process was known and constant for each experiment, the total volume of permanent gases produced was deduced, from the gas volume measured. The volume and mass of each gas species (H_2, CO, CO_2, CH_4) were then determined from the measured gas composition. As the repeatability was found to be satisfactory, the gas, liquid, and solid mass measured for the pyrolysis-only tests were subtracted from the gasification experiments to obtain the product yield associated only to the gasification stage. Under all the tested conditions, the mass balance closure for the gasification stage was in the range 88.6% and 103%, considered acceptable for the presented experimental setup. The gasification product yield as a function of the initial biomass and steam used in the pyro-gasification process was calculated according to Eqs. (1)–(3).

$$Char\ yield(\%) = \frac{m_{char}}{m_{biomass} + m_{steam}} \cdot 100 \tag{1}$$

$$Liquid\ yield(\%) = \frac{m_{liquid}}{m_{biomass} + m_{steam}} \cdot 100 \tag{2}$$

$$Gas\ yield(\%) = \frac{m_{gas}}{m_{biomass} + m_{steam}} \cdot 100 \tag{3}$$

where m_{char} is the mass of the recovered char at the end of the experiment, and m_{liquid} and m_{gas} are the mass of liquid and gas produced during the gasification stage. For their part, $m_{biomass}$ and m_{steam} are the mass of the initial biomass used and the steam fed to the gasification process. For the present study, the gasification total product yield with respect to the initial biomass is below 100%, as only the gasification products are considered in the calculation procedure.

For all the experimental conditions, the energy fraction associated to the gas, liquid, and solid by-products was determined. Their chemical energy, as well as their sensible or latent heat at the gasification temperature were taken into account, as presented below:

$$E_{prod} = E_{solid} + E_{gas} + E_{liquid} \tag{4}$$

$$E_{solid} = m_{char}\left(C_{pchar}T_r + HHV_{char}\right) \tag{5}$$

$$E_{gas} = m_{gas}\left(h_{gas(T_r)} + HHV_{gas}\right) \tag{6}$$

$$E_{liquid} = m_{steam}\left(h_{steam(T_r)}\right) + m_{tars}\left(h_{tars(T_r)} + HHV_{tars}\right) \tag{7}$$

where m_{char} and m_{gas} are the mass of the recovered char and gas at the end of the gasification process. $C_{p\ char}$ is the specific heat capacity of the char [36], and T_r is the reactor temperature during the gasification stage. For their part, h_{gas} is the enthalpy of the produced gas at temperature T_r leaving the gasifier, and h_{steam} is the enthalpy of the unreacted steam also at temperature T_r. Finally, HVV_{char} and HVV_{gas} are the high heating value of the recovered char and gas. As the mass of tars could not be accurately determined during the gasification stage, it is assumed for the liquid energy fraction calculation that the recovered liquids correspond only to unreacted steam. In accordance, the energy fraction of each gasification product was calculated according to Eqs. (8)–(10):

$$E.frac_{gas}(\%) = \frac{E_{gas}}{E_{prod}} \cdot 100 \tag{8}$$

$$E.frac_{char}(\%) = \frac{E_{char}}{E_{prod}} \cdot 100 \tag{9}$$

$$E.frac_{liquid}(\%) = \frac{E_{liquid}}{E_{prod}} \cdot 100 \tag{10}$$

Finally, considering the permanent gases as the targeted product, the gas efficiency of the gasification process is defined as follows:

$$Gas_{eff}(\%) = \frac{m_{gas} HHV_{gas}}{m_{biomass} HHV_{biomass} + m_{steam} h_{steam(T_r)}} \cdot 100 \quad (11)$$

where $m_{biomass}$ and m_{steam} are the mass of the initial biomass used and the total steam fed to the gasification process, HHV_{gas} and $HHV_{biomass}$ are the high heating value of the produced gas and the raw biomass, and $h_{steam\ (Tr)}$ is the enthalpy of the steam at the reactor temperature T_r during the gasification process.

2.4. Gasification reactivity analysis

To analyze the impact of the raw samples characteristics on their gasification behavior, an average reactivity study was performed for different gasification times. The conversion degree of the char after the gasification stage is defined as in Eq. (12):

$$\alpha(t) = \frac{m_0 - m(t)}{m_0 - m_{ash}} \quad (12)$$

where m_0 is the mass of the sample at the beginning of the gasification stage, $m(t)$ the mass at the end of the gasification period t, and m_{ash} the mass of ash in the sample. For each experimental condition m_0 is the mass of char in the reactor before the steam injection, determined from the pyrolysis-only tests. The apparent gasification reactivity is expressed as a function of the conversion degree α. In general, reactivity comparisons are referred to a specific sample conversion level. Nevertheless, considering that the continuous monitoring of the mass change was not possible in the presented experimental arrangement, the gasification reactivity is expressed in this study as the mean value calculated for a defined gasification time, as presented in Eq. (14), where t is the time of the steam gasification stage, from 1 h to 3 h.

$$R(\alpha)_{(app)} = \frac{1}{1-\alpha(t)} \frac{d\alpha}{dt} \quad (13)$$

$$R(\alpha)_{(app)average} = \frac{1}{n} \sum_{t=1}^{n} \frac{1}{1-\alpha(t)} \frac{d\alpha}{dt} \quad (14)$$

2.5. Chemical characterization of the steam gasification solid by-product

The local chemical composition of the samples at a micro-scale was analyzed using a Hitachi TM3030 Plus tabletop scanning electron microscope (SEM), with an energy dispersive X-ray spectroscopy (EDX) module in the same apparatus. For its part, elemental mapping of chemical species at a nano-scale was performed using a JEOL JEM-ARM200F transmission electron microscope (TEM) with energy dispersive X-ray spectroscopy (EDX) capability. The inorganic crystalline species present in the steam gasification biochars were identified using X-ray diffraction (XRD). The analysis in char powder samples (particle size below 250 μm) were carried out using a Phillips Panalyrical X'pert Pro MPD diffractometer using a Cu Ka radiation source (1.543 Å) with a current of 4 kV and an intensity of 40 mA. The diffraction patterns were collected between $2\theta = 10$ and $2\theta = 70$ with a step size of 0.05°.

Temperature programmed desorption measurements (TPD) were also performed in a Micromeritics AutoChem II chemisorption analyzer, to identify the presence of oxygen-containing functional groups in the solid by-product surface. Around 150 mg of sample were placed in a quartz U-tube and heated from 25 °C to 1000 °C at 5 °C/min, under a helium flow of 50 ml/min. The effluent gas was monitored using a MyGC Agilent micro-GC. Desorption experiments were performed twice, and their repeatability was found to be satisfactory, with a maximum calculated standard deviation below 10% for all the analyzed samples.

3. Results and discussion

3.1. Bioresources steam gasification reactivity and product yield

The steam gasification by-product distribution and the associated energy fractions were determined for the selected feedstocks: coconut shells (CS), bamboo guadua (BG), and oil palm shells (OPS). The experimental results showed that for the three samples, a rise in the gasification temperature resulted in an increase in the gas production and a decrease in the solid and liquid yields, as presented in Fig. 2. Indeed, with the temperature change from 750 °C to 850 °C, the gas yield after 1 h shifted from 0.50 to 0.94 g/g_{bio} (0.66 to 1.41 Nl/g_{bio}) for coconut shells (CS), from 0.47 to 0.54 g/g_{bio} (0.75 to 0.81 Nl/g_{bio}) for bamboo guadua (BG), and from 0.44 to 0.56 g/g_{bio} (0.79 to 0.84 Nl/g_{bio}) for oil palm shells (OPS). This is an augmentation of 18, 3 and 5 percentage points respectively, while the liquid and solid yields decreased for the three samples. The detailed experimental results are presented in Table 2.

This trend is associated with an increase in the steam gasification reactivity with the temperature. In particular, from the average values calculated for the analyzed samples, a reactivity increase of at least four times was observed with the temperature change from 750 °C to 850 °C, from 0.35, 0.25 and 0.08 to 2.28, 1.18 and 0.32 for coconut shells, bamboo guadua, and oil palm shells respectively. This general behavior was expected, considering that endothermic steam gasification reactions, especially the water gas reaction ($C + H_2O \rightarrow CO + H_2 + 131$ kJ/kmol), is promoted by higher temperatures, resulting in an enhanced gas production [13,19,24]. However, it is worth noting that even though the described trend is the same for the three samples, significant differences are observed. For the same gasification time, the increase in the gas production was greater for CS in comparison to OPS and BG, when the gasification temperature rose from 750 °C to 850 °C. Similarly, the energy fraction contained in the permanent gases augmented 28 percentage points for CS compared to only 10 and 5 for BG and OPS respectively (Fig. 2). The decrease in the energy fraction associated with the recovered solids and liquids was also greater for CS.

The experimental results proved that under the same gasification conditions the gas production evolution is also different for the three samples. Notably, CS exhibited the highest gas yield, while BG and OPS showed a similar behavior, as observed in Fig. 3. These differences are consistent with the calculated average reactivity values, revealing that regardless of the process temperature, the gasification reactivity of CS was always higher in comparison to BG and OPS. For instance, at 850 °C, the BG and OPS reactivities correspond to only 51% and 14% of the CS value respectively, clarifying the observed differences in the gas yield evolution with the gasification temperature and time. Accordingly, two different trends are identified: CS in one hand, with high steam gasification reactivity, and BG and OPS on the other hand.

Despite the differences in the macromolecular structure of the samples, the observed trend may be mainly related to their inherent inorganic content. For instance, CS and OPS showed very different gasification behavior despite their comparable macromolecular composition and nature (endocarp biomasses). In contrast, BG and OPS showed similar gas yield evolution under the same gasification conditions. Specifically, CS contain mainly K and Ca, while OPS and BG are principally composed of Si, Al, and P, as described in Table 1. On this subject, the beneficial effect of AAEM on the steam gasification behavior of carbon materials, as well as its inhibition by Si, Al, or P, has been highlighted by different authors [32,37,38], and kinetically confirmed in a previous work [26,39].

In the particular case of steam gasification, the influence of alkali and alkaline earth metals (AAEM) on the water gas reaction ($C + H_2O \rightarrow CO + H_2$) has been described as an oxygen transfer mechanism via the metal M, involving the reaction of salts with carbon, followed by the subsequent metal oxidation by the gaseous environment [40,41]. As a result, the enhanced oxygen exchange between the gasifying atmosphere and

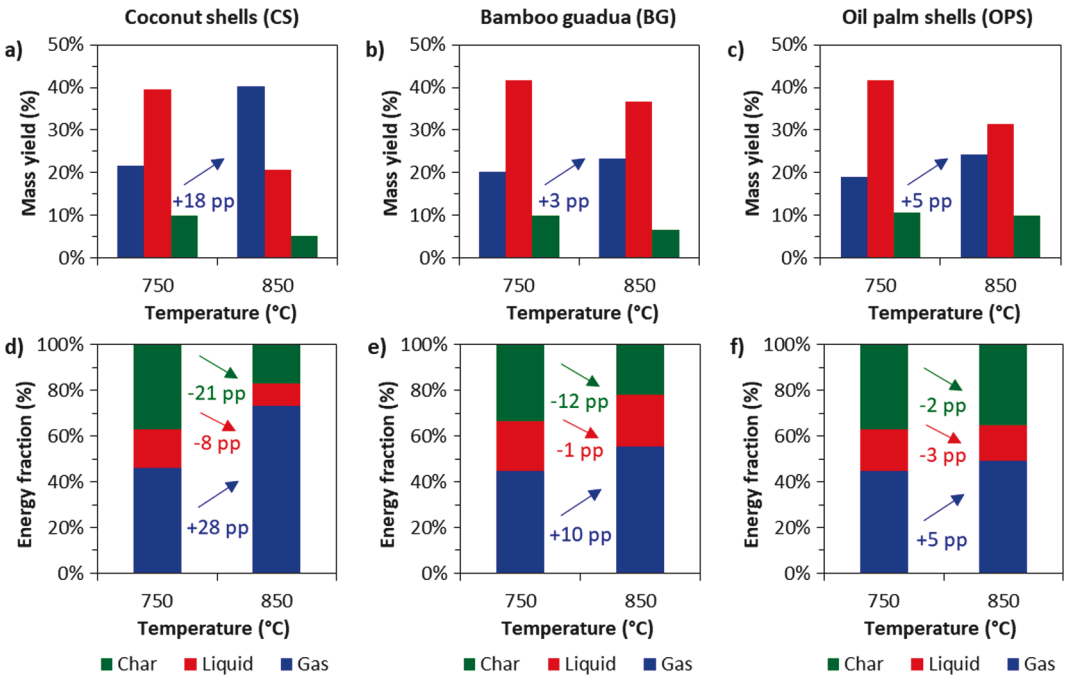

Fig. 2. Steam gasification product yield and associated energy fractions. a), b), c) product yield from steam gasification of coconut shells (CS), bamboo guadua (BG), and oil palm shells (OPS), at 750 °C and 850 °C during 1 h. d), e), f) energy fraction associated to the steam gasification by-products. (pp. percentage points).

Table 2
Steam gasification by-products distribution and associated energy fraction for the analyzed experimental conditions.

	Product distribution			Product energy fraction			Gas efficiency (%)
Raw sample [a]	Solid (g/g_{bio})	Liquid (g/g_{bio})	Gas (g/g_{bio})	Solid (%)	Liquid (%)	Gas (%)	
CS_750°C_1h	0.23	0.92	0.50	37.0%	17.0%	46.0%	33.2%
CS_750°C_2h	0.20	1.98	0.75	23.3%	30.6%	46.2%	37.1%
CS_750°C_3h	0.16	2.97	1.26	13.0%	32.6%	54.4%	52.0%
CS_850°C_1h	0.12	0.48	0.94	16.9%	10.1%	73.0%	54.6%
CS_850°C_2h	0.04	1.18	1.62	3.9%	15.4%	80.7%	78.3%
BG_750°C_1h	0.23	0.97	0.47	33.4%	21.9%	44.7%	31.0%
BG_750°C_2h	0.21	2.11	0.65	21.4%	34.4%	44.2%	34.4%
BG_750°C_3h	0.20	3.40	0.79	15.7%	43.9%	40.5%	33.6%
BG_850°C_1h	0.15	0.85	0.54	21.8%	22.9%	55.4%	33.3%
BG_850°C_2h	0.12	1.84	0.92	8.9%	31.4%	59.7%	45.3%
BG_850°C_3h	0.08	2.76	1.34	3.4%	34.5%	62.0%	53.8%
OPS_750°C_1h	0.25	0.97	0.44	37.1%	18.2%	44.8%	35.5%
OPS_750°C_2h	0.24	2.12	0.65	25.1%	27.1%	47.8%	45.9%
OPS_750°C_3h	0.24	3.11	0.88	19.4%	31.9%	48.7%	49.3%
OPS_850°C_1h	0.23	0.73	0.56	35.3%	15.5%	49.2%	35.1%
OPS_850°C_2h	0.20	1.62	1.00	19.8%	21.7%	58.5%	54.5%
OPS_850°C_3h	0.16	2.62	1.35	12.6%	27.4%	60.0%	60.3%
Blends [b]							
50%CS_50%BG	0.16	0.65	0.76	24.2%	13.7%	62.1%	46.5%
50%CS_50%OPS	0.17	0.72	0.73	27.4%	14.8%	57.8%	44.6%
90%CS_10%BG	0.15	0.46	0.89	22.6%	9.3%	68.1%	52.7%
90%CS_10%OPS	0.12	0.68	0.86	19.0%	14.1%	66.9%	51.2%

Analyzed samples: coconut shells (CS), bamboo guadua (BG), oil palm shells (OPS).
[a] Sample name gives information about gasification conditions: sample_temperature_time.
[b] Biomass blends were gasified at 850 °C, during 1 h.

the reacting solid increases the carbon conversion rate, leading to a higher reactivity and gas production (Fig. 4). This is the case of CS, considering that their main inorganic constituents are alkali and alkaline earth metals (around 3700 mg/kg dry basis). In accordance, this sample exhibits a catalytic gasification behavior, with a higher gas yield in comparison with the other two selected feedstocks.

However, the described catalytic mechanism may be inhibited by elements like Si, Al, and P, as they tend to react with AAEM, reducing their beneficial effect [26,32,33,39]. In particular, the formation of alkali phosphates, silicates, and aluminosilicates may hinder the oxygen transfer mechanism via the metal M, and in consequence, the catalytic impact of AAEM on the steam gasification reactions [42–44]. Despite the fact that BG and OPS have non-negligible amounts of AAEM (around 6000 and 1200 mg/kg dry basis respectively), the significant content of Si, Al, and P in these samples (around 20,400 and 7300 mg/kg dry basis respectively), may explain their similar behavior and the notable differences observed with CS. The catalytic steam gasification of CS and the inhibitory impact of Al, Si, and P was confirmed by the physico-chemical

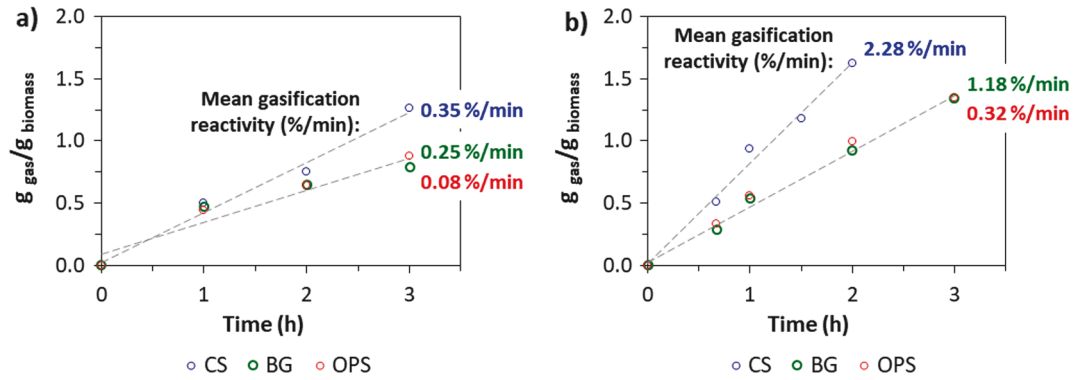

Fig. 3. Gas production evolution with the gasification time. a) Gasification temperature: 750 °C. b) Gasification temperature: 850 °C. The mean steam gasification reactivity values calculated for each sample at 750 °C and 850 °C are presented next to the corresponding gas production curve.

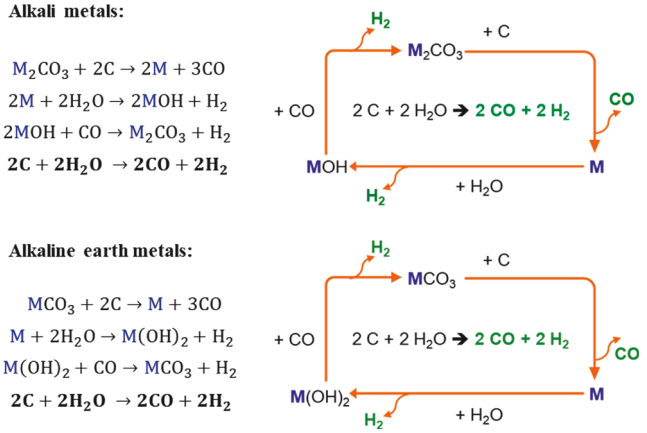

Fig. 4. Reaction mechanism of water–gas reaction ($C + H_2O \rightarrow CO + H_2$) in the presence of AAEM. The possible oxygen transfer mechanism between the gaseous atmosphere (H_2O) and the reacting solid (C) is schematized [38,40].

characterization of the process solid by-product.

3.2. *Catalytic gasification revealed by the process solid by-product*

The oxygen transfer mechanisms between the sample and the gasifying atmosphere may involve the intermediate creation of oxygen and hydrogen surface complexes in the reacting carbon substrate. In accordance, the characterization of the process solid by-product, also called *biochar,* corroborated the favorable effect of AAEM on the development of gasification reactions. In particular, the thermal programmed desorption (TPD) results revealed a higher extent of oxygen-containing surface complexes in the samples obtained from coconut shells, showing greater amounts of desorbed CO and CO_2 in all the analyzed TPD temperature range (25–800 °C), in comparison to the other two feedstocks (Fig. 5). In the case of samples from steam gasification at 850 °C during 1 h, the total amount of desorbed products for CS char was 1.5 and 3 times higher than the observed values for BG and OPS chars respectively (1.41 mmol/g compared to 0.95 mmol/g for BG and 0.48 mmol/g for OPS). Moreover, the observed differences in the total amount of CO and CO_2 desorption increased to 2.5 and 5 times respectively, for a gasification time of 2 h (2.32 mmol/g compared to 0.90 mmol/g for BG and 0.50 mmol/g for OPS). This behavior suggests an enhanced oxygen exchange between the carbon substrate and the gasifying agent for CS, and confirms the catalytic impact of AAEM on the development of steam gasification reactions, according to the mechanism described (see Fig. 4).

Moreover, the association of Si, the main inorganic constituent of BG and OPS, with the AAEM present in these samples, was verified by TEM-EDX and SEM-EDX analysis, confirming the chemical affinity of these elements under the studied steam gasification conditions, and in consequence, the inhibition of the presented catalytic reaction mechanism. From TEM-EDX cartographic images presented in Fig. 6a, it was possible to observe that Si may be present in the biochar as SiO_2, or associated to K or Ca. Furthermore, single point SEM-EDX spectra of BG and OPS biochars confirmed the presence of Si, P, and Al, and their association to AAEM, probably as phosphates, silicates, or aluminosilicates (Fig. 6b–d). In the particular case of BG biochar, the presence of calcium potassium phosphate $CaKPO_4$ (01-074-1951) and cristobalite SiO_2 (96-900-8230) was verified by XRD analysis (Fig. S1 in Supplementary Information. Other species like $KAlSiO_4$ (00-155-0184) may probably be present, but hidden by the intense SiO_2 peaks in XRD difractograms. In contrast, the occurrence of these compounds was not observed in coconut shells biochar samples.

3.3. *Prediction of bioresources steam gasification behavior*

From the experimental results and the described reaction mechanism, it is possible to conclude that the proportion of AAEM in relation to Si, Al, and P in the raw feedstocks, determines their steam gasification behavior. In this regard, different inorganic ratios were analyzed in order to establish their relationship with the gasification reactivity and product yield of lignocellulosic bioresources. In the first place, the ratio (Na + K + Na + Mg)/(Si + Al + P), considering the impact of the usual inherent AAEM in agrowastes, seems to appropriately describe the two observed trends: values higher than one indicate a catalytic gasification behavior of samples, contrary to values below one. However, considering that among AAEM, K has been identified as the most active element promoting the steam gasification reactions in carbon materials [28,29], the simplified inorganic ratio K/(Si + P) can be considered as a straightforward method to depict the gasification behavior of samples. The validity of the latter fraction, proposed by Hognon et al. [45], was kinetically confirmed in a previous study [26,34], and validated here as a way to predict the occurrence of a catalytic mechanism during the biomass steam gasification. It is worth noting that despite the fact that a certain amount of minerals may volatilize during the pyrolysis stage, high mineral retentions levels were observed in pyrolysis biochars for K, Si, and P (>80%) [46–48]. In accordance, the proposed inorganic ratio based on the raw biomass composition is a good indicator of the samples gasification behavior.

Regarding the analyzed raw samples, the inorganic ratio K/(Si + P) of coconut shells is 3.9, while bamboo guadua and oil palm shells values are 0.2 and 0.17 respectively. The clear differences observed between the samples, explain the outstanding behavior of coconut shells in relation to gas production and efficiency (see methods). Specifically, the process gas efficiency calculated for gasification at 850 °C, during 1 h, is around 20 percentage points higher for coconut shells, in comparison to

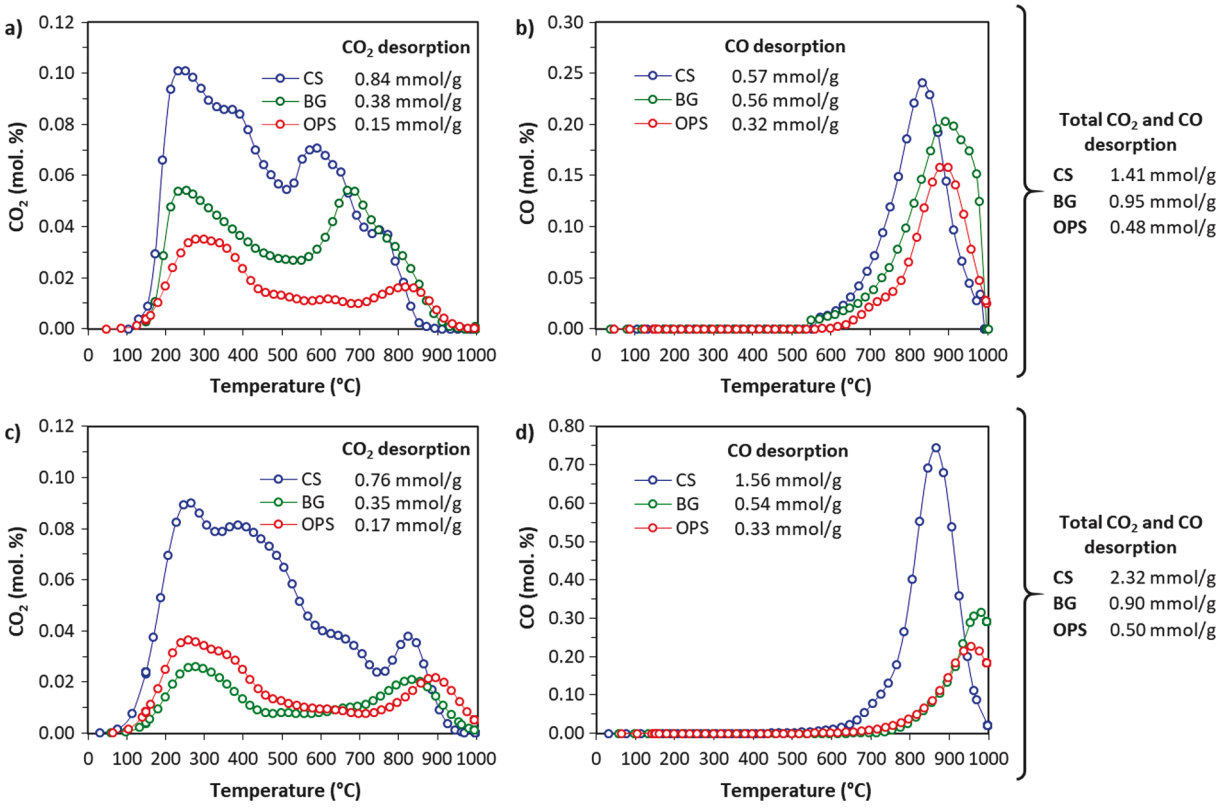

Fig. 5. Thermal programmed desorption analysis of steam gasification biochars. a), b) CO and CO_2 desorption of biochars from steam gasification of the three analyzed samples at 850 °C for 1 h (coconut shells (CS), bamboo guadua (BG) and oil palm shells (OPS)). c), d), CO and CO_2 desorption of biochars from steam gasification of the three analyzed samples at 850 °C for 2 h.

the values obtained for bamboo guadua and oil palm shells (55% in comparison to 33% and 35% respectively). In this regard, to further illustrate the influence of the inherent inorganic elements in the raw biomass, the gasification behavior, product yield, and process efficiency of selected biomass blends was also analyzed and compared. Under the same process conditions, two different trends were clearly distinguished (Fig. 7). In the first place, it can be noted that the gas efficiency of the process increases with K/(Si + P) for ratios below 1. In contrast, the highest gas efficiencies were observed for biomasses and blends with K/(Si + P) close to or higher than 1. It is worth noting that for samples with an inorganic ratio higher than 1, the calculated gas efficiency remained almost constant.

It should be mentioned that from the analysis of the gas yield and gas efficiency obtained for each sample, it is not possible to evidence synergistic or inhibitory effects as a function of the biomass blend ratio. However, the experimental results highlight the evolution of the gasification behavior of samples as a function of their inorganic ratio. These findings confirm the validity of the inorganic ratio K/(Si + P) adopted in this work to classify and predict the behavior of lignocellulosic agro-waste. From a practical point of view, this observation is particularly relevant for real applications, as the process parameters and conditions should be adapted according to the feedstock characteristics. In particular, longer gasification times or higher temperatures are required for biomasses with low gasification reactivity, identified by an inorganic ratio K/(Si + P) lower than 1. Moreover, the behavior of biomass blends may be estimated from the knowledge of the inorganic composition of the individual feedstocks.

3.4. Steam gasification fuel-gas composition

Despite the two different trends observed in the steam gasification behavior of the analyzed samples as a function of their inorganic composition, it is worth noting that no significant differences were identified in terms of the produced gas composition, as observed in Fig. 8. In fact, under the same gasification conditions, the catalytic development of the water–gas reaction ($C + H_2O \rightarrow CO + H_2$), associated to the presence of AAEM in the biomass, enhances the gas production, but does not show a significant effect in the produced gas composition, as detailed in Fig. 4. In all cases, H_2 was identified as the main gaseous species, with an average fraction near 60%, followed by CO and CO_2 with 19% and 18% respectively. Concentrations below 0.6% of CH_4 were also observed in all cases, and below 0.02% of C_2H_4 for OPS.

For the three samples, a slight decrease between 2 and 5 percentage points in the H_2 fraction was observed with the temperature rise from 750 °C to 850 °C. This behavior is probably related to the water–gas shift reaction ($CO + H_2O \rightarrow CO_2 + H_2$), that could be disfavored with the temperature increase. In fact, this reaction is slightly exothermic (-41 kJ/kmol), and has a higher equilibrium constant at lower temperatures, implying lower H_2 yields when the temperature increases [49–51]. The CH_4 content in the produced gas is very low, considering that methanation reactions ($C + 2H_2 \leftrightarrow CH_4$ −74.8 kJ/kmol, $2CO + 2H_2 \rightarrow CH_4 + CO_2$ −247 kJ/kmol, or $CO + 3H_2 \leftrightarrow CH_4 + H_2O$ −206 kJ/kmol) are not favored in the analyzed temperature range (exothermic reactions). In this regard, the slight decrease in the CH_4 content with the gasification temperature may be related to the equilibrium constant decrease of these reactions with temperature.

Under all the tested conditions, the calculated gas high heating value (HHV) was between 10 and 12 MJ/m^3, as expected for a steam gasification process of lignocellulosic materials (Supplementary Table S1) [15,16,52–54]. Moreover, the average H_2/CO ratio of the produced gas, with values between 2.5 and 4.5 suggests its suitability in energy applications, as fuel in gas turbines or internal combustion engines [55–57]. The similarities between the gas compositions obtained from

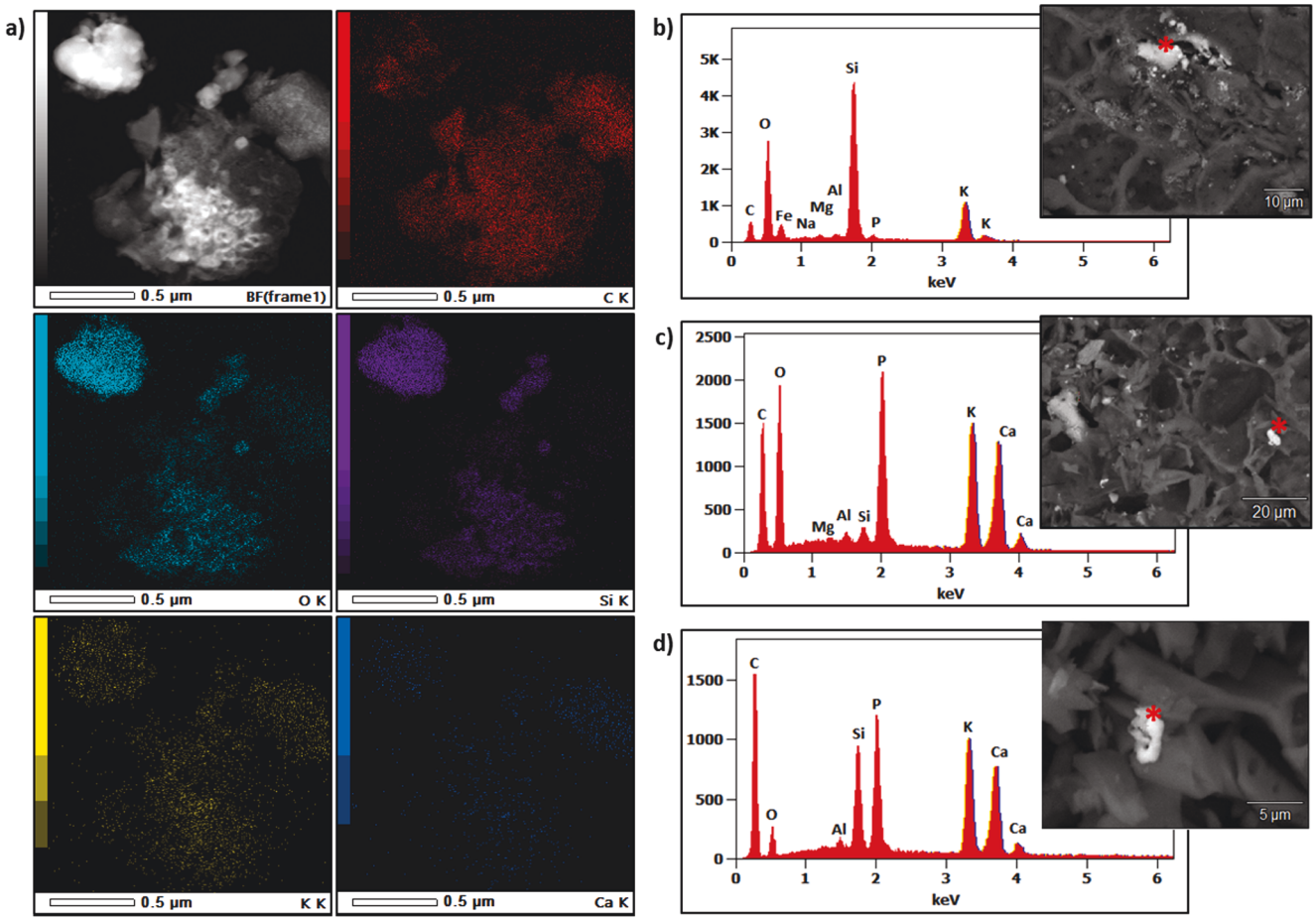

Fig. 6. Chemical characterization of steam gasification solid by-product. a) TEM-EDX images of biochar from the steam gasification of bamboo guadua (BG) at 850 °C during 1 h. b) SEM-EDX spectra corresponding biochar from the steam gasification of oil palm shells (OPS) at 850 °C during 1 h. c), d) SEM-EDX spectra corresponding to biochar from the steam gasification of bamboo guadua (BG) at 850 °C during 1 h.

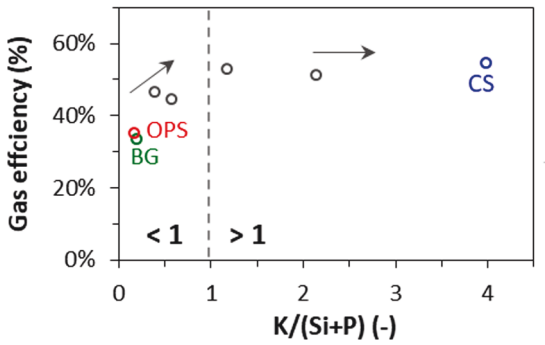

Biomass / blend	K/(Si+P)
100%CS	3.98
100%BG	0.20
100%OPS	0.17
90%CS 10%OPS	2.15
90%CS 10%BG	1.18
50%CS 50%OPS	0.58
50%CS 50%BG	0.39

Fig. 7. Process gas efficiency. The calculated process gas efficiency for pure samples and selected blends is compared at the same gasification conditions: 850 °C during 1 h. The average inorganic ratio K/(Si + P) of pure samples and blends is detailed.

the selected biomasses and blends may be mainly related to their close organic content, with H/C and O/C ratios near 1.5 and 0.8 respectively (Table 1). In this respect, Cao et al. [58] found a correlation between the H_2/CO ratio of the gasification gas and the H/C ratio of different range coals. Particularly, in the case of the analyzed raw biomasses, the H/C ratio is very close, as well as the H/C ratio of the pyrolysis biochars at the beginning of the gasification stage (0.15 for CS biochar, 0.16 for BG biochar, and 0.18 for OPS biochar at 850 °C), supporting the similar gas composition observed.

4. Conclusion

AAEM, and particularly K, have a catalytic effect on the steam gasification reactions of bioresources. It may be nevertheless inhibited by elements like Al, Si, and P. The gasification catalytic mechanism associated with the presence of AAEM in the raw biomass was described as the enhancement of the oxygen transfer mechanism between the carbon and the reacting atmosphere. Its inhibition by Si, Al, and P was confirmed by the characterization of the gasification solid by-product. Accordingly, this work confirms the validity of the inorganic ratio K/(Si + P) to predict the steam gasification reactivity and kinetics of

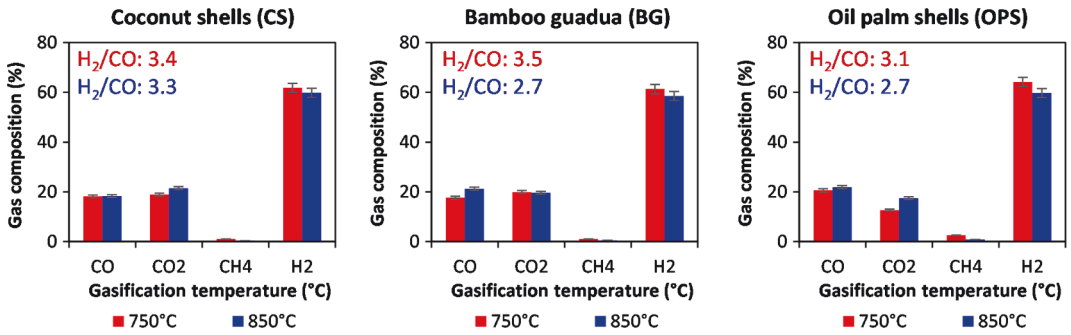

Fig. 8. Produced gas average composition. Steam gasification at 750 °C and 850 °C during 1 h.

bioresources, and demonstrates its strength to also predict their steam gasification performance, regarding energy applications. Specifically, the process product distribution and energy fractions. Under the same conditions, samples with K/(Si + P) above 1 exhibited a higher gas yield and efficiency in comparison to samples with K/(Si + P) below 1. This work depicts the mechanisms leading bioresources conversion, and constitutes and important reference to properly adapt the process parameters of gasification facilities to the feedstock characteristics and application requirements. The universality of the proposed inorganic ratio K/(Si + P) needs to be further analyzed in the future with other kinds of bioresources.

CRediT authorship contribution statement

Lina María Romero Millán: Conceptualization, Investigation, Methodology, Writing - original draft. **Fabio Emiro Sierra Vargas:** Conceptualization, Funding acquisition. **Ange Nzihou:** Conceptualization, Supervision, Funding acquisition.

Declaration of Competing Interest

The authors declare that they have no known competing financial interests or personal relationships that could have appeared to influence the work reported in this paper.

Acknowledgements

The funding support from the French Laboratory of Excellence in Science of Energy Conversion (Labex), with the grant ANR 10 LABX 22 is gratefully acknowledged. Also, the authors would like to thank COLCIENCIAS, for the doctoral scholarship awarded in the frame of the Colombian National Program for Doctoral Formation 647-2014.

Appendix A. Supplementary data

Supplementary data to this article can be found online at https://doi.org/10.1016/j.fuel.2020.119527.

References

[1] Foster C. Agricultural wastes. Charateristics, types and management. Nova Sci 2015.
[2] Danish WZ. Does biomass energy consumption help to control environmental pollution? Evidence from BRICS countries. Sci Total Environ 2019;670:1075–83. https://doi.org/10.1016/j.scitotenv.2019.03.268.
[3] Hiloidhari M, Bhuyan N, Gogoi N, Seth D, Garg A, Singh A, et al. Agroindustry wastes: biofuels and biomaterials feedstocks for sustainable rural development. Refin Biomass Residues Sustain Energy Bioprod 2020:357–88. https://doi.org/10.1016/B978-0-12-818996-2.00016-8.
[4] Lal R. World crop residues production and implications of its use as a biofuel. Environ Int 2005. https://doi.org/10.1016/j.envint.2004.09.005.
[5] Liu B, Rajagopal D. Life-cycle energy and climate benefits of energy recovery from wastes and biomass residues in the United States. Nat Energy 2019;4:700–8. https://doi.org/10.1038/s41560-019-0430-2.
[6] Martínez JD, Mahkamov K, Andrade RV, Silva Lora EE. Syngas production in downdraft biomass gasifiers and its application using internal combustion engines. Renew Energy 2012;38:1–9. https://doi.org/10.1016/j.renene.2011.07.035.
[7] Pereira EG, Da Silva JN, De Oliveira JL, MacHado CS. Sustainable energy: a review of gasification technologies. Renew Sustain Energy Rev 2012;16:4753–62. https://doi.org/10.1016/j.rser.2012.04.023.
[8] Pacioni TR, Soares D, Di DM, Rosa MF, de Moreira RFPM, José HJ. Bio-syngas production from agro-industrial biomass residues by steam gasification. Waste Manage 2016. https://doi.org/10.1016/j.wasman.2016.08.021.
[9] Ahmad FB, Zhang Z, Doherty WOS, O'Hara IM. The outlook of the production of advanced fuels and chemicals from integrated oil palm biomass biorefinery. Renew Sustain Energy Rev 2019;109:386–411. https://doi.org/10.1016/j.rser.2019.04.009.
[10] Zhou L, Martirez JMP, Finzel J, Zhang C, Swearer DF, Tian S, et al. Light-driven methane dry reforming with single atomic site antenna-reactor plasmonic photocatalysts. Nat Energy 2020. https://doi.org/10.1038/s41560-019-0517-9.
[11] Zhong L, Yu F, An Y, Zhao Y, Sun Y, Li Z, et al. Cobalt carbide nanoprisms for direct production of lower olefins from syngas. Nature 2016;538:84–7. https://doi.org/10.1038/nature19786.
[12] Lan W, Chen G, Zhu X, Wang X, Wang X, Xu B. Research on the characteristics of biomass gasification in a fluidized bed. J Energy Inst 2018. https://doi.org/10.1016/j.joei.2018.03.011.
[13] Yan F, Luo S-Y, Hu Z-Q, Xiao B, Cheng G. Hydrogen-rich gas production by steam gasification of char from biomass fast pyrolysis in a fixed-bed reactor: Influence of temperature and steam on hydrogen yield and syngas composition. Bioresour Technol 2010;101:5633–7. https://doi.org/10.1016/j.biortech.2010.02.025.
[14] Balu E, Lee U, Chung JN. High temperature steam gasification of woody biomass – A combined experimental and mathematical modeling approach. Int J Hydrogen Energy 2015;40:14104–15. https://doi.org/10.1016/j.ijhydene.2015.08.085.
[15] Pinto F, André R, Miranda M, Neves D, Varela F, Santos J. Effect of gasification agent on co-gasification of rice production wastes mixtures. Fuel 2016;180:407–16. https://doi.org/10.1016/j.fuel.2016.04.048.
[16] Fremaux S, Beheshti S-M, Ghassemi H, Shahsavan-Markadeh R. An experimental study on hydrogen-rich gas production via steam gasification of biomass in a research-scale fluidized bed. Energy Convers Manage 2015;91:427–32. https://doi.org/10.1016/j.enconman.2014.12.048.
[17] Karatas H, Akgun F. Experimental results of gasification of walnut shell and pistachio shell in a bubbling fluidized bed gasifier under air and steam atmospheres. Fuel 2018;214:285–92. https://doi.org/10.1016/j.fuel.2017.10.061.
[18] Yip K, Tian F, Hayashi J-I, Wu H. Effect of alkali and alkaline earth metallic species on biochar reactivity and syngas compositions during steam gasification. Energy Fuels 2010;24:173–81. https://doi.org/10.1021/ef900534n.
[19] Herguido J, Corella J, González-Saiz J. Steam gasification of lignocellulosic residues in a fluidized bed at a small pilot scale. Effect of the type of feedstock. Ind Eng Chem Res 1992;31:1274–82. https://doi.org/10.1021/ie00005a006.
[20] Sharma V, Kuila A. Lignocellulosic Biomass Production and Industrial Applications. Wiley; 2017.
[21] Bajpai P. Pretreatment of lignocellulosic biomass for biofuel production. vol. 34. 2016. doi:10.1007/978-981-10-0687-6.
[22] Niu W, Han L, Liu X, Huang G, Chen L, Xiao W, et al. Twenty-two compositional characterizations and theoretical energy potentials of extensively diversified China's crop residues. Energy 2016;100:238–50. https://doi.org/10.1016/j.energy.2016.01.093.
[23] Asadullah M, Zhang S, Min Z, Yimsiri P, Li C-Z. Effects of biomass char structure on its gasification reactivity. Bioresour Technol 2010;101:7935–43. https://doi.org/10.1016/j.biortech.2010.05.048.
[24] Guizani C, Sanz FJE, Salvador S. The gasification reactivity of high-heating-rate chars in single and mixed atmospheres of H2O and CO2. Fuel 2013;108:812–23. https://doi.org/10.1016/j.fuel.2013.02.027.
[25] Di Blasi C. Combustion and gasification rates of lignocellulosic chars. Prog Energy Combust Sci 2009;35:121–40. https://doi.org/10.1016/j.pecs.2008.08.001.
[26] Dupont C, Jacob S, Marrakchy KO, Hognon C, Grateau M, Labalette F, et al. How inorganic elements of biomass influence char steam gasification kinetics. Energy 2016;109:430–5. https://doi.org/10.1016/j.energy.2016.04.094.
[27] Bouraoui Z, Jeguirim M, Guizani C, Limousy L, Dupont C, Gadiou R. Thermogravimetric study on the influence of structural, textural and chemical

properties of biomass chars on CO2 gasification reactivity. Energy 2015;88:703–10. https://doi.org/10.1016/j.energy.2015.05.100.
[28] Perander M, Demartini N, Brink A, Kramb J, Karlström O, Hemming J, et al. Catalytic effect of Ca and K on CO 2 gasification of spruce wood char. Fuel 2015;150:464–72. https://doi.org/10.1016/j.fuel.2015.02.062.
[29] Huang Y, Yin X, Wu C, Wang C, Xie J, Zhou Z, et al. Effects of metal catalysts on CO 2 gasification reactivity of biomass char. Biotechnol Adv 2009;27:568–72. https://doi.org/10.1016/j.biotechadv.2009.04.013.
[30] Encinar JM, Gonzalez JF, Rodriguez JJ, Ramiro MJ. Catalysed and uncatalysed steam gasification of eucalyptus char: influence of variables and kinetic study. Fuel 2001;80:2025–36.
[31] Ferreira SD, Junges J, Scopel B, Manera C, Osório E, Lazzarotto IP, et al. Steam gasification of biochar derived from the pyrolysis of chrome-tanned leather shavings. Chem Eng Technol 2019;42:2530–8. https://doi.org/10.1002/ceat.201800660.
[32] Zhang Y, Ashizawa M, Kajitani S, Miura K. Proposal of a semi-empirical kinetic model to reconcile with gasification reactivity profiles of biomass chars. Fuel 2008;87:475–81. https://doi.org/10.1016/j.fuel.2007.04.026.
[33] Umeki K, Moilanen A, Gómez-Barea A, Konttinen J. A model of biomass char gasification describing the change in catalytic activity of ash. Chem Eng Technol 2012;207–208:616–24. https://doi.org/10.1016/j.cej.2012.07.025.
[34] Romero Millán LM, Sierra Vargas FE, Nzihou A. Steam gasification behavior of tropical agrowaste: a new modeling approach based on the inorganic composition. Fuel 2019;235:45–53. https://doi.org/10.1016/j.fuel.2018.07.053.
[35] CEN/TS 15439:2006. Biomass gasification - Tar and Particles in Product Gases – Sampling and Analysis. Brussels: 2006.
[36] Gupta M, Yang J, Roy C. Specific heat and thermal conductivity of softwood bark and softwood char particles☆. Fuel 2003;82:919–27. https://doi.org/10.1016/S0016-2361(02)00398-8.
[37] Kajita M, Kimura T, Norinaga K, Li C-Z, Hayashi J-I. Catalytic and Noncatalytic Mechanisms in Steam Gasification of Char from the Pyrolysis of Biomass 2009. doi:10.1021/ef900513a.
[38] Nzihou A, Stanmore B, Sharrock P. A review of catalysts for the gasification of biomass char, with some reference to coal. Energy 2013;58:305–17. https://doi.org/10.1016/j.energy.2013.05.057.
[39] Romero Millan LM, Sierra Vargas FE, Nzihou A. Catalytic effect of inorganic elements on steam gasification biochar properties from agrowastes. Energy Fuels 2019;33:8666–75. https://doi.org/10.1021/acs.energyfuels.9b01460.
[40] McKee DW. Mechanisms of the alkali metal catalysed gasification of carbon. Fuel 1983;62:170–5. https://doi.org/10.1016/0016-2361(83)90192-8.
[41] Mckee DW. Gasification of graphite in CO2 and water vapor- the catalytic effect of metal salts. Carbon N Y 1982;20:59–66.
[42] Boström D, Skoglund N, Grimm A, Boman C, Öhman M, Broström M, et al. Ash transformation chemistry during combustion of biomass. Energy Fuels 2012;26:85–93. https://doi.org/10.1021/ef201205b.
[43] Niu Y, Tan H, Hui S. Ash-related issues during biomass combustion: Alkali-induced slagging, silicate melt-induced slagging (ash fusion), agglomeration, corrosion, ash utilization, and related countermeasures. Prog Energy Combust Sci 2016;52:1–61. https://doi.org/10.1016/j.pecs.2015.09.003.
[44] Nutalapati D, Gupta R, Moghtaderi B, Wall TF. Assessing slagging and fouling during biomass combustion: a thermodynamic approach allowing for alkali/ash reactions. Fuel Process Technol 2007;88:1044–52. https://doi.org/10.1016/j.fuproc.2007.06.022.
[45] Hognon C, Dupont C, Grateau M, Delrue F. Comparison of steam gasification reactivity of algal and lignocellulosic biomass: influence of inorganic elements. Bioresour Technol 2014;164:347–53. https://doi.org/10.1016/j.biortech.2014.04.111.
[46] Ferreira S, Junges J, Reginato G, Lazzarotto I, Osorio E, Godinho M. Investigation of the structure of the biochar obtained by slow pyrolysis of elephant grass during its steam gasification. Chem Eng Technol 2019;42:2546–55. https://doi.org/10.1002/ceat.201800680.
[47] Romero Millán LM, Sierra Vargas FE, Nzihou A. Characterization of steam gasification biochars from lignocellulosic agrowaste towards soil applications. Waste Biomass Valorization 2020. https://doi.org/10.1007/s12649-020-01241-9.
[48] Keown DM, Favas G, Hayashi JI, Li CZ. Volatilisation of alkali and alkaline earth metallic species during the pyrolysis of biomass: differences between sugar cane bagasse and cane trash. Bioresour Technol 2005;96:1570–7. https://doi.org/10.1016/j.biortech.2004.12.014.
[49] Basu P. Biomass Gasification and Pyrolysis. Practical Design. First Edit. Oxford: Elsevier; 2010. doi:10.1016/B978-0-12-374988-8.00021-0.
[50] Butterman HC, Castaldi MJ. Influence of CO2 Injection on Biomass Gasification. Ind Eng Chem Res 2007;46:8875–86. https://doi.org/10.1021/ie071160n.
[51] Tristantini D, Supramono D, Suwignjo RK. Catalytic effect of K2CO3 in steam gasification of lignite char on mole ratio of H2/CO in syngas. Int J Technol 2015;6:22–30. https://doi.org/10.14716/ijtech.v6i1.208.
[52] Karatas H, Olgun H, Akgun F. Experimental results of gasification of cotton stalk and hazelnut shell in a bubbling fluidized bed gasifier under air and steam atmospheres. Fuel 2013;112:494–501. https://doi.org/10.1016/j.fuel.2013.04.025.
[53] Ahmed I, Gupta AK. Syngas yield during pyrolysis and steam gasification of paper. Appl Energy 2009;86:1813–21. https://doi.org/10.1016/j.apenergy.2009.01.025.
[54] Basu P. Biomass Gasification, Pyrolysis and Torrefaction (Second Edition) - Chapter 13 – Analytical Techniques. Second edi, Elsevier Inc.; 2013, p. 439–55.
[55] Butterman HC, Castaldi MJ. CO2 as a carbon neutral fuel source via enhanced biomass gasification. Environ Sci Technol 2009;43:9030–7. https://doi.org/10.1021/es901509n.
[56] Song X, Guo Z. Technologies for direct production of flexible H2/CO synthesis gas. Energy Convers Manage 2006;47:560–9. https://doi.org/10.1016/j.enconman.2005.05.012.
[57] Sahoo BB, Sahoo N, Saha UK. Effect of H 2:CO ratio in syngas on the performance of a dual fuel diesel engine operation. Appl Therm Eng 2012;49:139–46. https://doi.org/10.1016/j.applthermaleng.2011.08.021.
[58] Cao Y, Gao Z, Jin J, Zhou H, Cohron M, Zhao H, et al. Synthesis gas production with an adjustable H2/CO ratio through the coal gasification process: effects of coal ranks and methane addition. Energy Fuels 2008;22:1720–30. https://doi.org/10.1021/ef7005707.
[59] Romero Millan LM, Sierra Vargas FE, Nzihou A. Kinetic analysis of tropical lignocellulosic agrowaste pyrolysis. BioEnergy Res 2017;10:832–45. https://doi.org/10.1007/s12155-017-9844-5.